Knott, T.R., Branney, M.J., Reichow, M.K., Finn, D.R., Coe, R.S., Storey, M., Barfod, D., and McCurry, M., 2016, Mid-Miocene record of large-scale Snake River–type explosive volcanism and associated subsidence on the Yellowstone hotspot track: The Cassia Formation of Idaho, USA: GSA Bulletin, doi:10.1130/B31324.1.

## Analytical methods and data interpretations

Supplementary tables

# WHOLE ROCK X-RAY FLUORESCENCE (XRF) METHODOLOGY, UNIVERSITY OF LEICESTER, UK

Whole rock samples were prepared for major and trace element analysis by grinding in a Retsch planetary mill using agate pots and grinding balls. Major and trace element data were obtained on fusion beads and pressed powder pellets, respectively by X-ray fluorescence (XRF) analysis using a PANalytical Axios Advanced X-ray fluorescence spectrometer at the University of Leicester, UK. The PANalytical Axios runs a 4Kw Rhodium anode end window ceramic technology X-ray tube. Total loss on ignition (LOI) was measured on pre-dried powders after ignition at 950 °C in air for 1 h. Instrumental conditions have been selected to avoid any significant line overlaps within the usual compositional range of most geological materials. Stability of the current generation X-Ray Spectrometry systems is such that measurements are no longer ratioed to a monitor sample to minimise instrumental drift effects but selected suitable drift monitoring samples are analyzed at the commencement of each analytical run. Calibrations for major and trace element analyses were set using international rock reference material (e.g., BCR-1, BHVO-1, W-2; Table S5a-b) under the same conditions and regressing the measured count ratios against the recommended concentrations principally from Govindaraju (1994), Imai et al. (1995, 1996, 1999) and values published on the GeoREM reference site, utilizing the Philips based Fundamental parameters correction technique. The analyses of international reference material indicate that precision for the observed data range and over the period of analytical work was 1% and 5% or better for trace and major elements, respectively (Tables S5a and S5b).

# ELECTRON MICROPROBE METHODOLOGY, OPEN UNIVERSITY, MILTON KEYNES, UK

Thin sections (30 microns) were cut from select samples of each member of the Cassia Formation, and these were subsequently polished and carbon-coated prior to electron microprobe analysis.

Analyses of pyroxene phenocrysts were obtained at the Open University, Milton Keynes using a Cameca SX100 electron microprobe. An operating voltage of 20 kV and probe current of 20 nA (measured on a Faraday cage) with a 10 micron beam diameter were used for quantitative analysis. Data were reduced using the PAP correction routine of Pouchou and Pichoir (1985).

# <sup>40</sup>AR/<sup>39</sup>AR METHODOLOGY: QUATERNARY DATING LABORATORY (QUADLAB), NATURAL HISTORY MUSEUM OF DENMARK

 $^{40}$ Ar/ $^{39}$ Ar experiments were conducted on single sanidine crystals representing the Wooden Shoe Butte, the Big Bluff and Magpie Basin members, with Fish Canyon sanidine (FCs) as the neutron fluence monitor, using the age of  $28.172 \pm 0.028$  Ma (Rivera et al., 2011) and  $^{40}$ K

Knott, T.R., Branney, M.J., Reichow, M.K., Finn, D.R., Coe, R.S., Storey, M., Barfod, D., and McCurry, M., 2016, Mid-Miocene record of large-scale Snake River–type explosive volcanism and associated subsidence on the Yellowstone hotspot track: The Cassia Formation of Idaho, USA: GSA Bulletin, doi:10.1130/B31324.1.

decay constants of Min et al. (2000). Handpicked crystals of unknowns and FCs were loaded into 21-pit aluminum irradiation disks, wrapped in aluminum foil and heat-sealed within a quartz glass tube. Irradiation was conducted at the cadmium-lined Oregon State University TRIGA reactor during two separate irradiations with irradiation times of 20 and 16 h, respectively. Single sanidine crystal <sup>40</sup>Ar/<sup>39</sup>Ar laser fusion analyses were carried out on a Nu Instruments Noblesse noble gas mass spectrometer that is equipped with one faraday and three ETP multiplier (ioncounting) detectors housed at the Quaternary Dating Laboratory (QUADLAB), Natural History Museum of Denmark, following methods similar to those detailed by Brumm et al. (2010). Crystals were gently degassed prior to fusion using a defocused beam from a 50 W Synrad CO<sub>2</sub> laser, followed by total fusion at 4–12 W power with a focused beam. Analyses of unknowns, blanks and monitor minerals were carried out in identical fashion, by measuring <sup>40</sup>Ar and <sup>39</sup>Ar on the single (high-mass) faraday detector (F), <sup>38</sup>Ar and <sup>37</sup>Ar on the axial ion counter, and <sup>36</sup>Ar on the low-mass ion counter, with baselines measured every cycle. Measurement of the <sup>40</sup>Ar, <sup>38</sup>Ar and <sup>36</sup>Ar ion beams was carried out simultaneously and followed by measurement of <sup>39</sup>Ar and then the <sup>37</sup>Ar beam. Beam switching was achieved by varying the field of the mass spectrometer magnet and with minor adjustment of the quad lenses. All signals measured on the ion counters are dead-time corrected. Observed <sup>40</sup>Ar/<sup>36</sup>Ar and <sup>40</sup>Ar/<sup>38</sup>Ar ratios were corrected for instrument mass fractionation and detector efficiencies using correction factors calculated for each detectorisotope combination, using a time series of measured blank-corrected air aliquots derived from a calibrated air pipette relative to published atmospheric ratios  $({}^{40}\text{Ar}/{}^{36}\text{Ar})_{A} = 298.56$  and  $({}^{40}\text{Ar}/{}^{38}\text{Ar})_{\text{A}} = 1583.7$  (Lee et al., 2006). Corrections for interfering isotopes produced by nucleogenic reactions during the irradiation were based on Renne et al. (2005) with the exception of the value used for  $({}^{36}\text{Ar}/{}^{37}\text{Ar})_{Ca} = (2.646 \pm 0.008) \times 10^{-4}$ . Data collection and reduction were carried out using the program MASS SPEC (A. Deino, Berkeley Geochronology Centre). Jvalues were calculated for the irradiation positions of the FCs for the irradiation disk and the  $^{40}$ Ar\*/ $^{39}$ Ar<sub>K</sub> ratio of the FC<sub>S</sub> extrapolated to the axial position of the unknowns using a planefitting algorithm. This  ${}^{40}\text{Ar}*/{}^{39}\text{Ar}_{\text{K}}$  ratio was used to calculate the J-values for the unknowns. Relative Ar-isotope abundances for samples given in the supplementary data table are blank and decay corrected and given in volts (Table S3). Outlier detection of individual <sup>40</sup>Ar/<sup>39</sup>Ar age data within each data population are determined when the normalized median absolute deviation (nMAD) is greater than 1.5 (Powell et al., 2002).

#### Results

#### Wooden Shoe Member (basal vitrophyre sample RC-10.1–002; Lab. ID. 2483)

Twenty-seven single crystal laser fusion experiments on sanidine feldspar (250–500  $\mu$ m) of the Wooden Shoe Butte Member sample RC-10.1–002 were conducted relative to Fish Canyon sanidine monitor minerals. Wooden Shoe Butte Member sanidine were highly radiogenic with 40Ar\* >90% (Figure S1a). The single crystal experiments yielded reproducible ages providing a weighted mean age of 10.139 ± 0.006 Ma (MSWD = 1.07; n = 21 of 27) for this member, which is statistically consistent with the inverse isochron age (10.141 ± 0.007 Ma; MSWD = 1). Regression of the data provides a <sup>40</sup>Ar/<sup>36</sup>Ar intercept of 295 ± 8 which is in good agreement with the published atmospheric ratio (Lee et al., 2006) and along with consistent Ca/K ratios (Table S3). Cumulative probability distribution of our data suggests a slight age zonation, implying the presence of three age populations (10.136 Ma, 10.155 Ma and 10.215 Ma) of which

Knott, T.R., Branney, M.J., Reichow, M.K., Finn, D.R., Coe, R.S., Storey, M., Barfod, D., and McCurry, M., 2016, Mid-Miocene record of large-scale Snake River–type explosive volcanism and associated subsidence on the Yellowstone hotspot track: The Cassia Formation of Idaho, USA: GSA Bulletin, doi:10.1130/B31324.1.

only the latter two are statistically different from our weighted mean age. The observed age distribution is interpreted to result from the presence of antecryst sanidine possibly recycled from a previous magmatic episode. We therefore consider the weighted mean age with an acceptable MSWD, which excludes the youngest and the five oldest sanidine ages, to represent the best estimate of the crystallization age. Our new age is younger than the previously published age of  $10.25 \pm 0.06$  Ma (recalculated to the same FCs monitor age of  $28.172 \pm 0.028$  Ma obtained by Rivera et al., 2011) derived from multi-grain experiments for this member (Perkins et al., 1995). As for the Big Bluff Member above, the identification of older sanidine crystals in our Wooden Shoe Butte ignimbrite single grain experiments are interpreted to be the most likely cause for the observed age difference.

#### Big Bluff Member (basal vitrophyre sample RC-10.1–011; Lab ID. 2443)

Thirty-six single crystal laser fusion experiments on sanidine feldspar (250–500 µm) of the Big Bluff Member sample RC-10.1–011 were conducted relative to the Fish Canyon sanidine monitor. Big Bluff Member sanidines are highly radiogenic with 40Ar\* typically >90% with one experiment providing a slightly lower 40Ar\* yield of 88% (Figure S1b). The single crystal experiments yielded reproducible ages providing a weighted mean age of 10.952 ± 0.010 Ma (MSWD = 0.91; n = 31 of 36) for this member. The weighted mean age is statistically consistent with the inverse isochron age of 10.952 ± 0.018 Ma (MSWD = 1). Regression of the data provide a <sup>40</sup>Ar/<sup>36</sup>Ar intercept of 298 ± 11 which is in good agreement with the published atmospheric ratio (298.56 ± 0.31; Lee et al., 2006) and along with consistent Ca/K ratios (Table S3) indicate only one source of radiogenic argon. Cumulative probability distribution of our data implies the presence of which one is statistically distinct sanidine (11.641 ± 0.014 Ma; Table S3) possibly recycled from a previous magmatic episode. We consider the weighted mean age as the most reliable estimate of crystallization.

Our new weighted mean age of  $10.952 \pm 0.010$  Ma (Figure S1b) for this member is statistically indistinguishable from the (recalculated to FCs monitor at  $28.172 \pm 0.028$  Ma; Rivera et al., 2011) sanidine argon age of  $10.97 \pm 0.07$  Ma by Ellis et al. (2012). However, our new age differs from an older age of  $11.05 \pm 0.03$  Ma derived from multi-grain (2–3) experiments for this member (Perkins et al., 1995). The identification of older sanidine crystals in our single grain experiments of the Big Bluff ignimbrite and, when incorporated into multigrain experiments, is the most likely cause for this difference.

#### Magpie Basin Member (basal vitrophyre sample MP-11.2–001; Lab ID. 2459)

The Magpie Basin Member sanidine (250–500  $\mu$ m) measurements yield a normal distribution with a weighted mean age of 11.337 ± 0.008 Ma (MSWD 1.43) including sixty-five of eighty single crystal laser fusion experiments (Figure S1c). All sanidine were, except for two analyses, highly radiogenic with 40Ar\* >90%. This result is statistically in good agreement with the inverse isochron age of 11.336 ± 0.009 Ma (MSWD = 1) and the corresponding <sup>40</sup>Ar/<sup>36</sup>Ar intercept of 294 ± 11 along with consistent Ca/K ratios (Table S3) indicate only one source of radiogenic argon and an atmospheric trapped argon composition. However, cumulative probability distribution of our data suggests a subtle age zonation, implying the presence of older, probably inherited grains. We interpret these data similar to those obtained on the Wooden Shoe above, to represent sanidine with extended pre-eruptive residence or possibly antecryst recycled from a previous magmatic episode. The weighted mean age, which is statistically

Knott, T.R., Branney, M.J., Reichow, M.K., Finn, D.R., Coe, R.S., Storey, M., Barfod, D., and McCurry, M., 2016, Mid-Miocene record of large-scale Snake River–type explosive volcanism and associated subsidence on the Yellowstone hotspot track: The Cassia Formation of Idaho, USA: GSA Bulletin, doi:10.1130/B31324.1.

indistinguishable from the inverse isochron age, is considered to represent the best estimate of the crystallization age for the Magpie Basin Member.

#### <sup>40</sup>AR/<sup>39</sup>AR METHODOLOGY: SCOTTISH UNIVERSITIES ENVIRONMENTAL RESEARCH CENTRE (SUERC), EAST KILBRIDE, SCOTLAND

Feldspars were separated for argon geochronology from rhyolitic members of the Cassia Formation using standard magnetic separation techniques. These feldspars were then handpicked in order to avoid those with significant alteration and or inclusions that could affect analyses.

Samples and neutron flux monitors (Fish Canyon Sanidine) were placed in aluminum discs and stacked in quartz tubes. The relative positions of wells in the discs were precisely measured for later reconstruction of neutron flux gradients. The sample package was irradiated for 8 h in the Oregon State University reactor, Cd-shielded facility. Fish Canyon Sanidine  $(28.172 \pm 0.028 \text{ Ma}; \text{Rivera et al., 2011})$  was used to monitor <sup>39</sup>Ar production and establish neutron flux values (J) for the samples and using the <sup>40</sup>K decay constants of Min et al. (2000). The neutron flux within a given disc is calculated by least-squares fitting of a surface to the J-monitors. Estimated errors in the neutron flux measurements are calculated from the residual deviation from the fitted surface.

Gas was extracted from samples using a mid-infrared CO<sub>2</sub> laser, with samples housed in a ZnS-window laser cell. Individual sample grains were loaded into a steel planchette containing 208 two millimeter diameter wells. Liberated argon was then purified of active gases (e.g., CO<sub>2</sub>, H<sub>2</sub>O, H<sub>2</sub>, N<sub>2</sub>, CH<sub>4</sub>) using three Zr-Ti-Al getters; one at 25 °C and two at 400 °C. Argon isotope ratios (i.e., ion beam intensities) were measured using a MAP 215–50 mass spectrometer in peak jumping mode. The mass spectrometer has a measured sensitivity of  $1.13 \times 10^{-13}$  mol/volt. Both the extraction and clean-up processes were automated, as were the mass spectrometer peak jumping routines and data acquisition. Time-intensity data are regressed to t<sub>0</sub> with second-order polynomial fits to the data. Mass discrimination was monitored by comparison to runningaverage values of an air standard. The average total system blank for laser extractions, measured once for every two unknowns, was  $2.5 \pm 0.3 \times 10^{-16}$  mol <sup>40</sup>Ar,  $2.5 \pm 0.4 \times 10^{-17}$  mol <sup>39</sup>Ar,  $9.6 \pm$  $2.1 \times 10^{-18}$  mol <sup>36</sup>Ar (1 $\sigma$  over the temperature range where age information is extracted. All data are blank and interference corrected and are displayed on ideograms (Figs. S2a-i). The mass discrimination correction assumes a value of 298.56 ± 0.31 (1 $\sigma$ ) for atmospheric argon (Lee et al., 2006; Mark et al., 2011).

#### Results

Crystal fusion experiments ( $\geq$ 36 individual crystals per sample) were conducted on 9 samples recovered from the Shoshone Falls Rhyolite, and the Kimberly, Castleford Crossing, Lincoln Reservoir, and Dry Gulch members. In general, data obtained on single plagioclase and sanidine feldspars provide reproducible ages though the range in radiogenic yield (<sup>40</sup>Ar\*) is in several cases large (e.g., Fig. S2f). Some plagioclase data are close to the limit of detection and together with very low (<50%) <sup>40</sup>Ar\* yields resulted in age calculations with increased uncertainties. Plagioclase with low radiogenic yields (<50%) and outliers with older ages (xenocrysts) present in each sample were omitted from the final age calculation. Nevertheless,

Knott, T.R., Branney, M.J., Reichow, M.K., Finn, D.R., Coe, R.S., Storey, M., Barfod, D., and McCurry, M., 2016, Mid-Miocene record of large-scale Snake River–type explosive volcanism and associated subsidence on the Yellowstone hotspot track: The Cassia Formation of Idaho, USA: GSA Bulletin, doi:10.1130/B31324.1.

the presented plagioclase ages suggest a sensible relation based on stratigraphic position of the selected samples and published ages of potentially related units (e.g., Honjo et al., 1986). The analyses, age-probability distribution plots, K/Ca ratios and radiogenic <sup>40</sup>Ar-yield for each experiment including calculated weighted mean ages are shown in Figures S2a-S2i. Data used for the calculation of mean ages were cast on isotope correlation plots; inverse isochrons overlap with the ages from the ideograms and <sup>40</sup>Ar/<sup>36</sup>Ar trapped components correspond with the accepted air value (Lee et al., 2006).

#### Shoshone Falls Rhyolite (Sample A2 751.6–754; Lab ID: EK65DB19)

Laser fusion experiments on Shoshone Falls Rhyolite single plagioclase (Fig. S2a) provided a statistically robust weighted mean age of  $6.37 \pm 0.22$  Ma (1 $\sigma$ ; MSWD = 0.67; n = 26 of 37). An older (~29 Ma), xenocrystic grain, is clearly identified in this sample. We consider our age to represent the best age of crystallization and age of the Shoshone Falls Rhyolite, which excludes xenocrystic grains and plagioclase with low radiogenic yield. Armstrong et al. (1975) report a younger whole rock K-Ar age of  $5.7 \pm 0.1$  Ma for the Shoshone Falls rhyolite. Similar  $^{40}$ Ar/ $^{39}$ Ar age results of  $6.53 \pm 0.04$  Ma (whole rock) and  $5.98 \pm 0.34$  Ma (plagioclase) for this member are also reported by Othberg et al. (2012). Unfortunately, the monitor used and its recommended age are not provided by the latter authors, and it remains unclear how these results compare to our new age.

#### **Kimberly Member**

Laser fusion experiments on single sanidine feldspar from samples A2–1419–1424 and A2–1945–1953 provided weighted mean ages of  $8.109 \pm 0.023$  Ma (1 $\sigma$ ; MSWD = 0.71; 22 of 36, Fig. S2b) and 7.951  $\pm$  0.055 Ma (1 $\sigma$ ; MSWD = 0.25; 24 of 37), respectively. The observed age distribution in plagioclase experiments from sample A2–1945–1953 (Fig. S2c) suggests the presence of multiple feldspar populations. Some ages older than the weighted mean age of this sample suggest derivation from a subjacent mid-Miocene ignimbrite presumably entrained in the magma chamber or during emplacement. However, age data with low radiogenic yield also provide younger ages implying the presence of argon loss. Although a statistically meaningful age for sample A2–1945–1953 was obtained, the age derived from the stratigraphically higher sample (A2–1419–1424) is considered to be more reliable.

#### Castleford Crossing Member

Two laser fusion experiments on single plagioclase feldspar were conducted on widespaced samples (Table S1) obtained from the Castleford Crossing Member. Laser fusion experiments on sample A2–2102–2106 (Figs S2d) provided a statistically meaningful weighted mean age of  $7.93 \pm 0.24$  Ma (1 $\sigma$ ; MSWD = 0.26; 30 of 37), whereas data obtained in the laser fusion experiment of sample MBH-12.2–013 provided a more complex age distribution (Fig S2e). Data of the latter sample plotted as age-probability distribution, provide evidence for the presence of older (~14 Ma ~21 and ~28 Ma) xenocrystic feldspars and a weighted mean age of  $8.10 \pm 0.21$  Ma (MSWD = 0.45; 20 of 37). Although both ages are statistically indistinguishable, we consider the age derived from sample A2–2102–2106 due to its lower MSWD, high statistical probability and generally higher radiogenic yields (>56%) as the best age for this

Knott, T.R., Branney, M.J., Reichow, M.K., Finn, D.R., Coe, R.S., Storey, M., Barfod, D., and McCurry, M., 2016, Mid-Miocene record of large-scale Snake River–type explosive volcanism and associated subsidence on the Yellowstone hotspot track: The Cassia Formation of Idaho, USA: GSA Bulletin, doi:10.1130/B31324.1.

member. However, both ages are younger than the published K-Ar age of  $9.15 \pm 0.13$  Ma obtained by Honjo et al. (1986).

#### Lincoln Reservoir Member

Cumulative probability distribution of data obtained on two Lincoln Reservoir Member samples (Figs. S2f and S2 g) demonstrate, similar to the Castleford Crossing Member, a broad and complex age distribution implying the presence of older, probably inherited grains. Although two statistically meaningful and indistinguishable ages of  $8.69 \pm 0.45$  Ma ( $1\sigma$ ; MSWD = 0.23) and  $7.97 \pm 0.16$  Ma ( $1\sigma$ ; MSWD = 0.48) were obtained from both experiments, low radiogenic yields (between 5% and 98%) may be responsible for the large uncertainties in these experiments. We conservatively consider the age obtained on sample RC-10.1–008 (Lab ID: EK65DB09) with its lower MSWD and higher probability as the best age for this member. However, a more precise age estimate preferentially by the U-Pb method on zircon for this member is required.

#### Dry Gulch Member

Experiments conducted on single plagioclase feldspars from two samples of the Dry Gulch Member provided statistically indistinguishable weighted mean ages of  $8.63 \pm 0.25$  Ma (1s; MSWD = 0.12, 32 of 37) and  $8.47 \pm 0.09$  Ma (1s; MSWD = 0.41, 31 of 37). Data with low radiogenic yields and from xenocrystic grains were rejected. These ages are also indistinguishable from those obtained on the stratigraphically younger Lincoln Reservoir, Castleford Crossing and Kimberly members. Although, our experiments provide statistically robust results, age data with higher resolution, preferentially by the U-Pb method on zircon are required to refine the age of this member.

#### U-PB ZIRCON GEOCHRONOLOGY—METHODOLOGY, EDINBURGH ION MICROPROBE FACILITY (EIMF), EDINBURGH, SCOTLAND

Zircons occurring in vitrophyre glass as free crystals, and as inclusions in ferromagnesian minerals were separated from basal vitrophyre of rhyolitic ignimbrites using standard heavy liquid and magnetic separation techniques. The majority of recovered zircons, regardless of size, are euhedral tetragonal dipyramids varying in length between 30–200  $\mu$ m. Rhyolites with smaller quantities of zircon have smaller grains (e.g., Indian Springs Member). Zircon grains were mounted in epoxy along with fragments of the reference zircon GJ-1. U-Pb dating of zircons was performed at the Edinburgh Ion Microprobe Facility (EIMF) using the CAMECA IMS-1270 ion microprobe.

A primary ion beam of ~5 nA <sup>16</sup>O2- created a beam diameter of ~25  $\mu$ m and rastered over 15  $\mu$ m<sup>2</sup> for two minutes to pre-clean the analysis area. The epoxy sample block was held under a vacuum and the surface was flooded with oxygen in order to double the yield of secondary Pb ions. A single electron multiplier was used in ion-counting mode to measure secondary ion beam intensities. Sputtered <sup>206</sup>Pb<sup>+</sup> ion yields, calculated from measurements on reference zircons of known Pb concentration, ranged from 20 - 36 cps/ppm <sup>206</sup>Pb<sup>+</sup> /nA primary beam (equivalent to 5 - 9 cps/ppm for an O-beam with no oxygen flooding). The Th/U ratio was determined using ThO/UO ratio measured on the 91500 standard twice each day (fractionation of

Knott, T.R., Branney, M.J., Reichow, M.K., Finn, D.R., Coe, R.S., Storey, M., Barfod, D., and McCurry, M., 2016, Mid-Miocene record of large-scale Snake River–type explosive volcanism and associated subsidence on the Yellowstone hotspot track: The Cassia Formation of Idaho, USA: GSA Bulletin, doi:10.1130/B31324.1.

the ThO/UO ratio from the absolute value was ~4–5%.). The internal reference zircon GJ-1, of known age 609 Ma (Jackson et al., 2004) was used to determine accurate U and Pb ion yields and measured after every 4 unknown analyses. All standards in a single session were averaged (minimum of 7 standards). A linear regression was applied (Kelly et al., 2008) to account for variations in U/Pb ratios, due to changes in instrument conditions. Instrumental mass fractionation was assumed to be 2 per mil per mass unit (based on previous measurements of glass standards). Total analytical time per spot was 27 min, pre sputtering (2 min), automatic centering of secondary ions (1 min), and analysis (24 min). From the GJ-1 standard we obtain an average  $^{207}$ Pb/<sup>206</sup>Pb ratio of 0.05993 ± 0.00011, which corresponds to an age of 604.1 ± 4.1 (2 $\sigma$ ; 57 repeats).

Correction for in situ common lead (surface contamination) has been made by measuring the amount of <sup>204</sup>Pb present and using a Stacey and Kramers (1975) estimation of terrestrial lead isotopic composition of modern day age. In addition the first 5 cycles during each spot analysis were omitted from any final age determinations. Only ages where common lead corrections were less than 3% were accepted (typically equivalent to >0.3 ppb <sup>204</sup>Pb). Corrections for Th/U disequilibria were made assuming mineral to whole rock ratio of 0.11 by assuming a bulk rock Th/U ratio of 4 and using the average zircon Th/U ratio of 0.5. The largest corrections for <sup>206</sup>Pb losses due to initial <sup>230</sup>Th depletion were less than 1.3% with most being close to 1%. The corrections for common Pb on mass <sup>207</sup>Pb are larger than they are for <sup>206</sup>Pb due to greater abundances of the <sup>206</sup>Pb isotope in zircon and possibly responsible for the slightly reversely discordant patterns of data. To arrive at the best age for each sample we have taken the weighted mean of the <sup>206</sup>Pb/<sup>238</sup>U zircon ages excluding analyses interpreted as having Pb loss.

#### Results

Fifty-eight ion microprobe analyses from three rhyolitic members of the Cassia formation are presented in Table S4. Zircons with common lead concentrations >6ppb <sup>204</sup>Pb were not used in age calculations and accompanying U-Pb Concordia diagrams (Fig. S3), and are thus not reported in Table S4. In general, high Pb concentrations (>20 ppm) are usually observed in xenocrystic zircons with Proterozoic ages but a correlation between U and Th content and zircon age are not observed. Although, statistically meaningful weighted mean <sup>206</sup>Pb/<sup>238</sup>U zircon ages could be derived from the three samples the presence of older zircons derived from subjacent mid-Miocene ignimbrites presumably entrained in the magma chamber or during emplacement cannot be ruled out. However, the resolution of data presented here precludes a more detailed account.

#### McMullen Creek Member (sample RC-10.1–006)

 $^{206}$ Pb/ $^{238}$ U zircon ages for the McMullen Creek Member range between 8.5 and 1414 Ma. However, 22 data points form a cluster of data with a weighted mean  $^{206}$ Pb/ $^{238}$ U age of 9.0 ± 0.2 Ma (MSWD = 2.3). Core analyses of zircon McM2–19 provided two Proterozoic ages of 1459 ± 4 and 1462 ± 12 Ma. Although, the  $^{206}$ Pb/ $^{238}$ U and  $^{206}$ Pb/ $^{207}$ Pb ages for analyses McM2–19–1 are not within uncertainty both  $^{206}$ Pb/ $^{207}$ Pb ages are in agreement and are considered to represent the crystallization age for this zircon. The rim analysis of zircon McM2–19 is clearly younger with a  $^{206}$ Pb/ $^{238}$ U age of 8.3 ± 0.2 Ma.

Knott, T.R., Branney, M.J., Reichow, M.K., Finn, D.R., Coe, R.S., Storey, M., Barfod, D., and McCurry, M., 2016, Mid-Miocene record of large-scale Snake River–type explosive volcanism and associated subsidence on the Yellowstone hotspot track: The Cassia Formation of Idaho, USA: GSA Bulletin, doi:10.1130/B31324.1.

#### Indian Springs Member (sample RC-10.1–010)

Analyses of zircons from the stratigraphically older Indian Springs Member sample provided a mean weighted  $^{206}$ Pb/ $^{238}$ U zircon ages of 9.0 ± 0.3 Ma (MSWD = 1.4; 9 out of 9 analyses; Table S4 and Figure S3b). This age is statistically indistinguishable from that obtained from the overlaying McMullen Creek Member.

#### Little Creek Member (sample RC-11.1–004)

Zircons from the Little Creek Member provide  ${}^{206}$ Pb/ ${}^{238}$ U ages between 9.3 and 11.0 Ma, though two zircon grains are with  ${}^{206}$ Pb/ ${}^{207}$ Pb ages ~1456 Ma clearly xenocrystic in origin (Table S4). Although a statistically meaningful weighted mean  ${}^{206}$ Pb/ ${}^{238}$ U age of 10.3 ± 0.2 Ma (MSWD = 3.1) can be derived for this sample (Fig. S3c) the age-probability distribution of these data imply the presence of two age populations at ~10.1 Ma and ~10.6 Ma (Fig. S3d). Furthermore, we obtained a high precision  ${}^{40}$ Ar/ ${}^{39}$ Ar sanidine age of 10.136 ± 0.005 Ma on the underlying Wooden Shoe Member (Fig. S1a). Although, the U-Pb and argon ages are, within uncertainties, indistinguishable the high-precision argon age from the underlying member provides a maximum age for the Little Creek Member, which consequently has to be younger.

## PALAEOMAGNETIC METHODOLOGY UNIVERSITY OF CALIFORNIA, SANTA CRUZ, USA

Laboratory work was conducted at the University of California, Santa Cruz, USA. Magnetic remanence measurement and automated progressive AF demagnetization up to 200 mT was performed on a 2G cryogenic magnetometer and Sapphire Instruments demagnetizer using a customized sample handler and software (Morris et al., 2009). Thermal demagnetization was carried out in a custom built oven housed in a magnetically shielded room along with the AF demagnetizer and cryogenic magnetometer. Fisher statistics (Fisher, 1953) and principal component analysis (Kirschvink, 1980) were used to average individual sample directions and to calculate the best fit lines to demagnetization data, respectively.

#### **REFERENCES CITED**

- Armstrong, R.L., Leeman, W.P., and Malde, H.E., 1975, K-Ar dating, quaternary and Neogene volcanic rocks of the Snake River Plain, Idaho: American Journal of Science, v. 275, p. 225–251, doi:10.2475/ajs.275.3.225.
- Brumm, A., Jensen, G.M., van den Bergh, G.D., Morwood, M.J., Kurniawan, I., Aziz, F., and Storey, M., 2010, Hominins on Flores, Indonesia, by one million years ago: Nature, v. 464, p. 748–752, doi:10.1038/nature08844.
- Ellis, B.S., Branney, M.J., Barry, T.L., Barfod, D., Bindeman, I., Wolff, J.A., and Bonnichsen, B., 2012, Geochemical correlation of three large-volume ignimbrites from the Yellowstone hotspot track, Idaho, USA: Bulletin of Volcanology, v. 74, p. 261–277, doi:10.1007/s00445-011-0510-z.
- Fisher, R.A., 1953, Dispersion on a sphere: Royal Society of London Proceedings, v. 217, p. 295–305, doi:10.1098/rspa.1953.0064.

Knott, T.R., Branney, M.J., Reichow, M.K., Finn, D.R., Coe, R.S., Storey, M., Barfod, D., and McCurry, M., 2016, Mid-Miocene record of large-scale Snake River–type explosive volcanism and associated subsidence on the Yellowstone hotspot track: The Cassia Formation of Idaho, USA: GSA Bulletin, doi:10.1130/B31324.1.

- Govindaraju, K., 1994, 1994 compilation of working values and sample description for 383 geostandards: Geostandards Newsletter, v. 18, p. 1–158, doi:10.1111/j.1751-908X.1994.tb00502.x.
- Honjo, N., McElwee, K.R., Duncan, R.A., Leeman, W.P., 1986, K-Ar ages of volcanic rocks from the Magic Reservoir eruptive centre, Snake River Plain, Idaho. Isochron/West, v. 46, p. 15–17.
- Imai, N., Terashima, S., Itoh, S., and Ando, A., 1995, 1994 compilation of analytical data for minor and trace elements in seventeen GSJ geochemical reference samples, "Igneous rock series: Geostandards Newsletter, v. 19, p. 135–213, doi:10.1111/j.1751-908X.1995.tb00158.x.
- Imai, N., Terashima, S., Itoh, S., and Ando, A., 1996, 1996 compilation of analytical data on nine GSJ geochemical reference samples, "Sedimentary rock series: Geostandards Newsletter, v. 20, p. 165–216, doi:10.1111/j.1751-908X.1996.tb00184.x.
- Imai, N., Terashima, S., Itoh, S., and Ando, A., 1999, 1998 compilation of analytical data for five GSL geochemical reference samples, the "Instrumental analysis series": Geostandards Newsletter, v. 23, p. 223–250, doi:10.1111/j.1751-908X.1999.tb00576.x.
- Jackson, S.E., Pearson, N.J., Griffin, W.L., and Belousova, E.A., 2004, The application of laser ablation-inductively coupled plasma-mass spectrometry to in situ U–Pb zircon geochronology: Chemical Geology, v. 211, p. 47–69, doi:10.1016/j.chemgeo.2004.06.017.
- Kelly, N.M., Hinton, R.W., Harley, S.L., and Appleby, S.K., 2008, New SIMS U–Pb zircon ages from the Langavat Belt, South Harris, NW Scotland: implications for the Lewisian Terrane mode: Journal of the Geological Society, v. 165, p. 967–981, doi:10.1144/0016-76492007-116.
- Kirschvink, J.L., 1980, The least-squares line and plane and the analysis of paleomagnetic data: Geophysical Journal of the Royal Astronomical Society, v. 62, p. 699–718, doi:10.1111/j.1365-246X.1980.tb02601.x.
- Lee, J.Y., Marti, K., Severinghaus, J.P., Kawamura, K., Yoo, H.S., Lee, J.B., and Kim, J.S., 2006, A redetermination of the isotopic abundances of atmospheric Ar: Geochimica et Cosmochimica Acta, v. 70, p. 4507–4512, doi:10.1016/j.gca.2006.06.1563.
- Mark, D.F., Stuart, F.M., and de Podesta, M., 2011, New high precision measurements for the isotopic composition of argon: Geochimica et Cosmochimica Acta, v. 75, p. 7494–7501, doi:10.1016/j.gca.2011.09.042.
- Min, K., Mundil, R., Renne, P.R., and Ludwig, K.R., 2000, A test for systematic errors in <sup>40</sup>Ar/<sup>39</sup>Ar geochronology through comparison with U/Pb analysis of a 1.1-Ga rhyolite: Geochimica et Cosmochimica Acta, v. 64, p. 73–98, doi:10.1016/S0016-7037(99)00204-5.
- Morris, E.R., Schillinger, W., Coe, R.S., Pluhar, C.J., and Jarboe, N.A., 2009, Automating the 2G superconducting rock magnetometer for single-solenoid alternating field demagnetization: Geochemistry Geophysics Geosystems, v. 10, doi:10.1029/2008GC002289.
- Othberg, K.L., Kauffman, J.D., Gillerman, V.S., and Garwood, D.L., 2012, Geologic Map of the Twin Falls 30 × 60 Minute Quadrangle, Idaho: Idaho Geological Survey, Morrill Hall University of Idaho Moscow, scale 1:100,000.
- Perkins, M.E., Nash, W.P., Brown, F.H., and Fleck, R.J., 1995, Fallout tuffs of Trapper Creek Idaho - a record of Miocene explosive volcanism in the Snake River Plain volcanic

Knott, T.R., Branney, M.J., Reichow, M.K., Finn, D.R., Coe, R.S., Storey, M., Barfod, D., and McCurry, M., 2016, Mid-Miocene record of large-scale Snake River–type explosive volcanism and associated subsidence on the Yellowstone hotspot track: The Cassia Formation of Idaho, USA: GSA Bulletin, doi:10.1130/B31324.1.

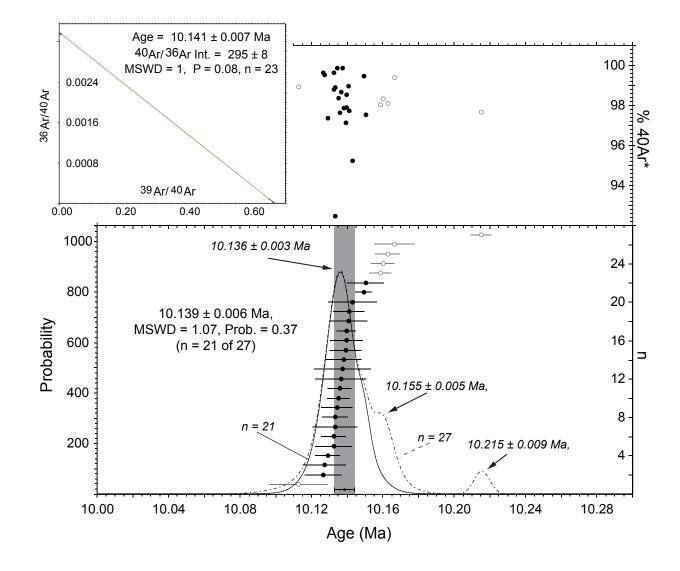
province: Geological Society of America Bulletin, v. 107, p. 1484–1506, doi:10.1130/0016-7606(1995)107<1484:FTOTCI>2.3.CO;2.

- Pouchou, J.L., and Pichoir, F., 1985, "PAP" procedure for improved quantitative analysis: Microbeam Analysis, v. 20, p. 104–105.
- Powell, R., Hergt, J., and Woodhead, J., 2002, Improving isochron calculations with robust statistics and the bootstrap: Chemical Geology, v. 185, p. 191–204, doi:10.1016/S0009-2541(01)00403-X.
- Renne, P.R., Knight, K.B., Nomade, S., Leung, K.-N., and Lou, T.-P., 2005, Application of deuteron–deuteron (D–D) fusion neutrons to 40Ar/39Ar geochronology: Applied Radiation and Isotopes, v. 62, p. 25–32, doi:10.1016/j.apradiso.2004.06.004.
- Rivera, T.A., Storey, M., Zeeden, C., Hilgen, F.J., and Kuiper, K., 2011, A refined astronomically calibrated <sup>40</sup>Ar/<sup>39</sup>Ar age for Fish Canyon sanidine: Earth and Planetary Science Letters, v. 311, p. 420–426, doi:10.1016/j.epsl.2011.09.017.
- Stacey, J.S., and Kramers, J.D., 1975, Approximation of terrestrial lead isotope evolution by a two-stage model: Earth and Planetary Science Letters, v. 26, p. 207–221, doi:10.1016/0012-821X(75)90088-6.

Figure S1. <sup>40</sup>Ar/<sup>39</sup>Ar single sanidine age probability distribution and percent <sup>40</sup>Ar\* (radiogenic) of (A) the Wooden Shoe; (B) the Big Bluff and c: the Magpie Basin members. Open symbols indicate outliers, and solid and dashed lines probability distribution excluding and including outliers, respectively. Individual analyses are shown with one-sigma errors and the weighted mean age with two-sigma uncertainty is indicated by gray bar. <sup>39</sup>Ar/<sup>40</sup>Ar inverse isochron diagram (inset).

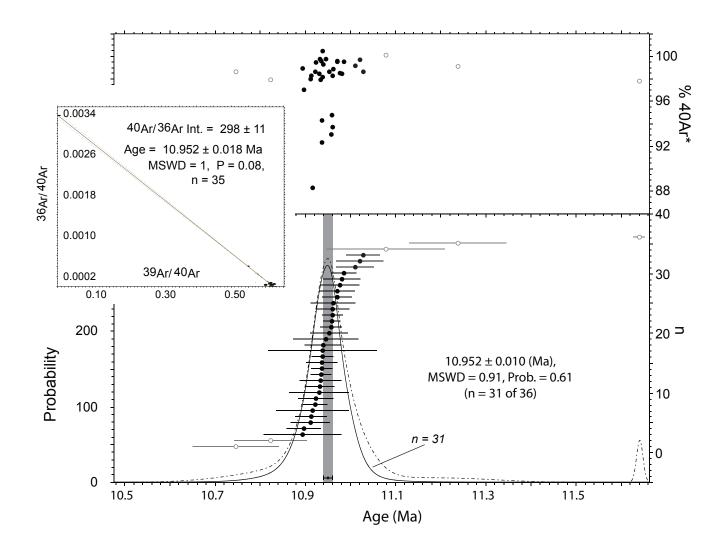
Figure S2. <sup>40</sup>Ar/<sup>39</sup>Ar single sanidine age probability distribution (ideograms) and percent <sup>40</sup>Ar\* (radiogenic) of: (A) Shoshone Rhyolite; (B–C) Kimberly Member; (D–E) Castleford Member; (F–G) Lincoln Reservoir Member; (H–I) Dry Gulch Member. Open symbols indicate outliers, and solid and dashed lines probability distribution excluding and including outliers, respectively. Individual analyses are shown with one-sigma errors and the weighted mean age with two-sigma uncertainty is indicated.

Figure S3. Concordia diagrams and weighted average plot for zircon 206Pb/238U ages for: (A) the McMullen Creek Member, (B) the Indian Springs Member, (C) the Little Creek Member. (D) Age-probability distribution plot of the Little Creek Member implying the presence of two age populations at ~10.1 Ma and ~10.6 Ma.



## Figure S1a; Wooden Shoe Member (ID 2483)





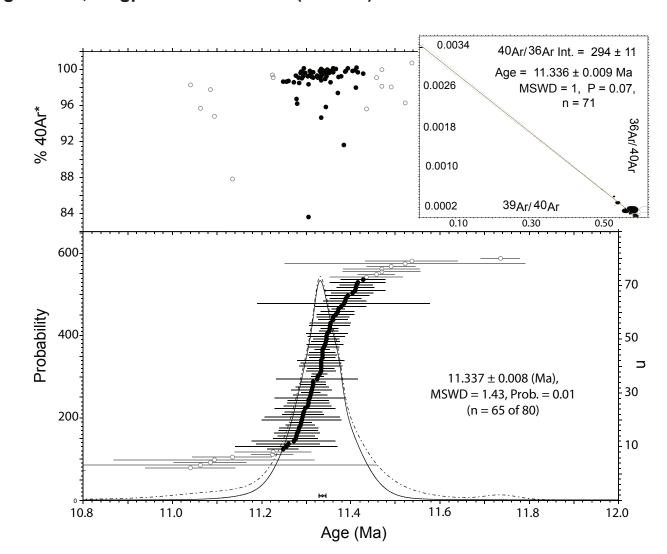
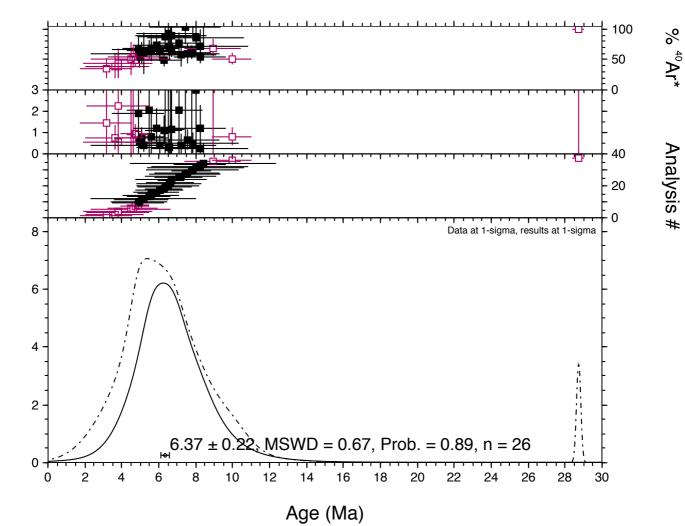


## Figure S1c; Magpie Basin Member (ID 2459)



K/Ca

Probability



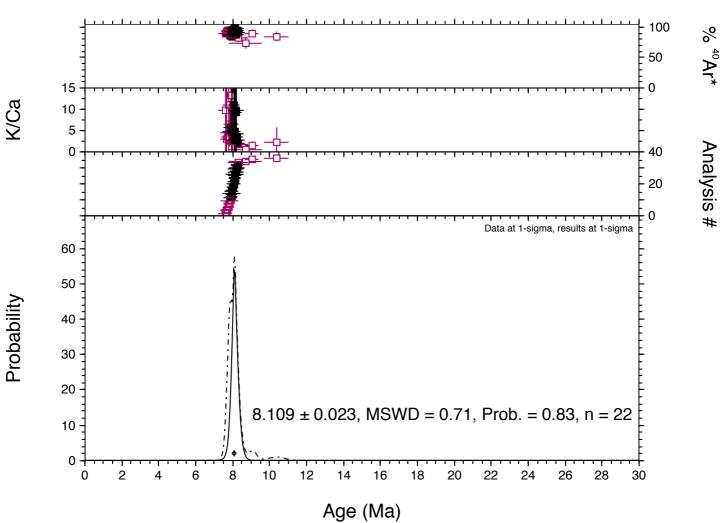


Figure S2b: Kimberly Member (ID EK65DB22)

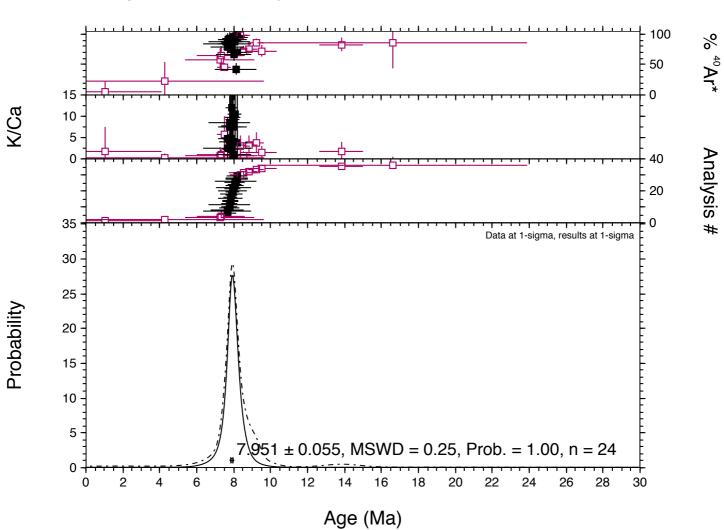


Figure S2c: Kimberly Member (ID EK65DB21)

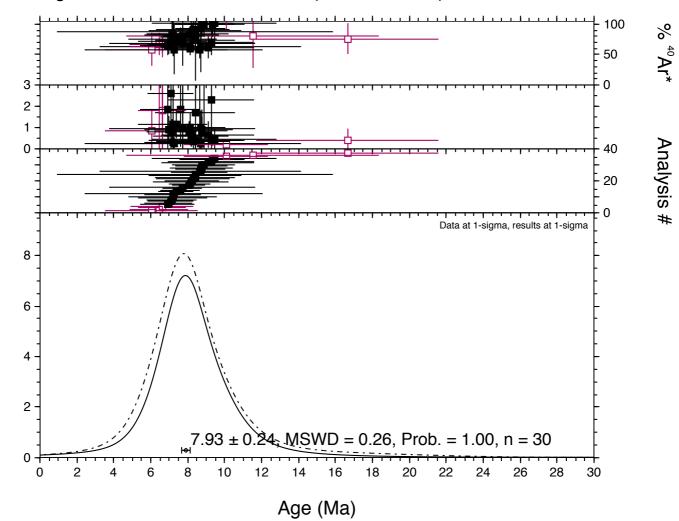
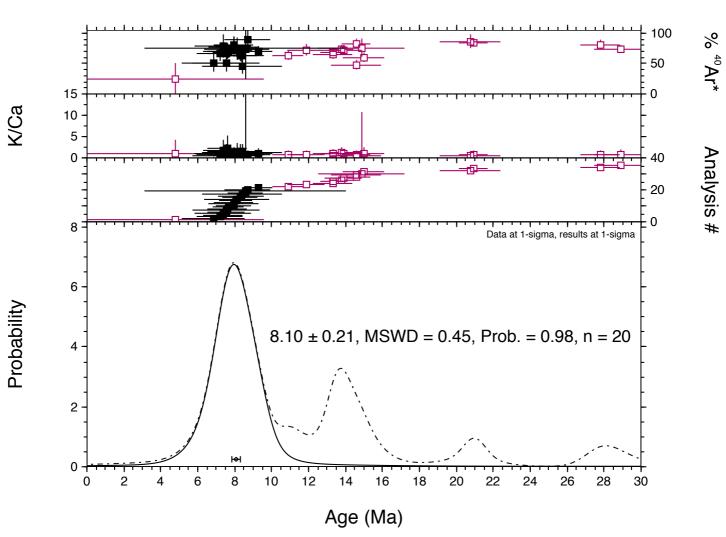


Figure S2d: Castleford Member (ID EK65DB20)

K/Ca

Probability





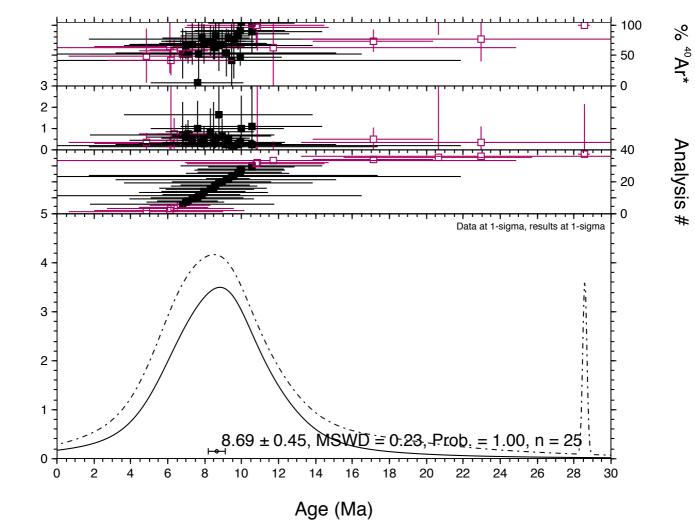
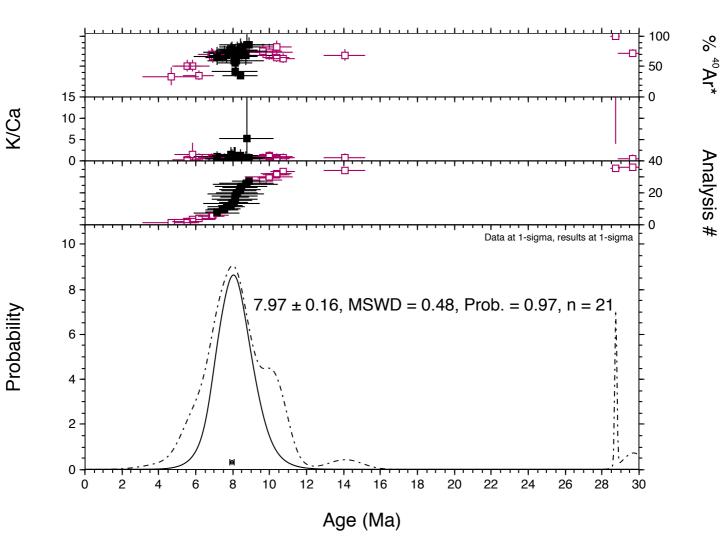


Figure S2f: Lincoln Reservoir Member (ID EK65DB09:RC-10.1-008)

Probability

K/Ca

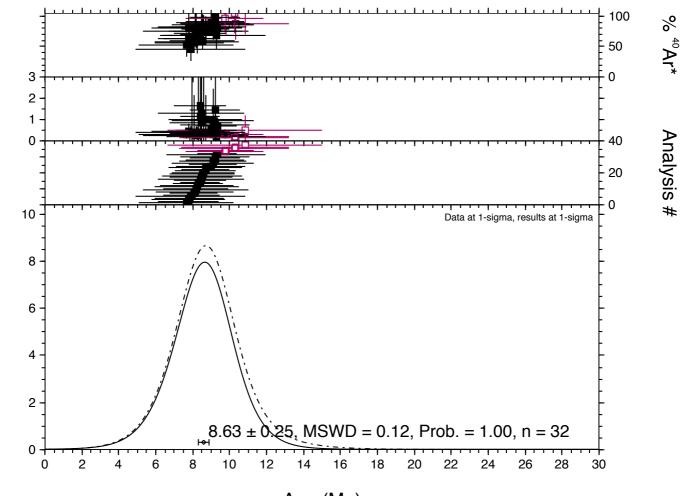




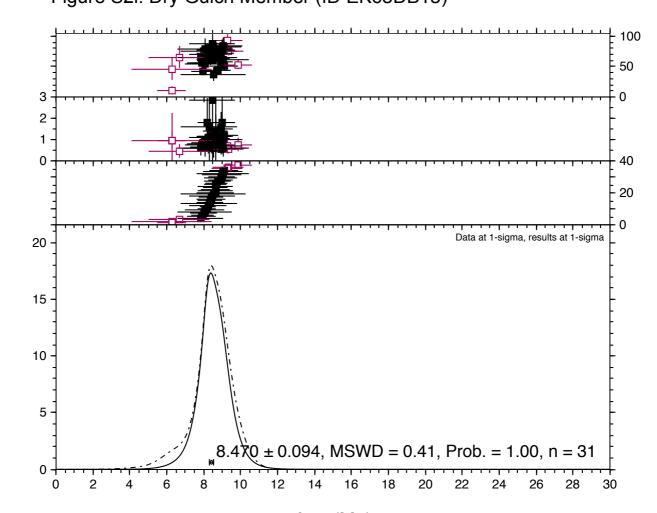


K/Ca

Probability



Age (Ma)



%  $^{40}$ Ar\*

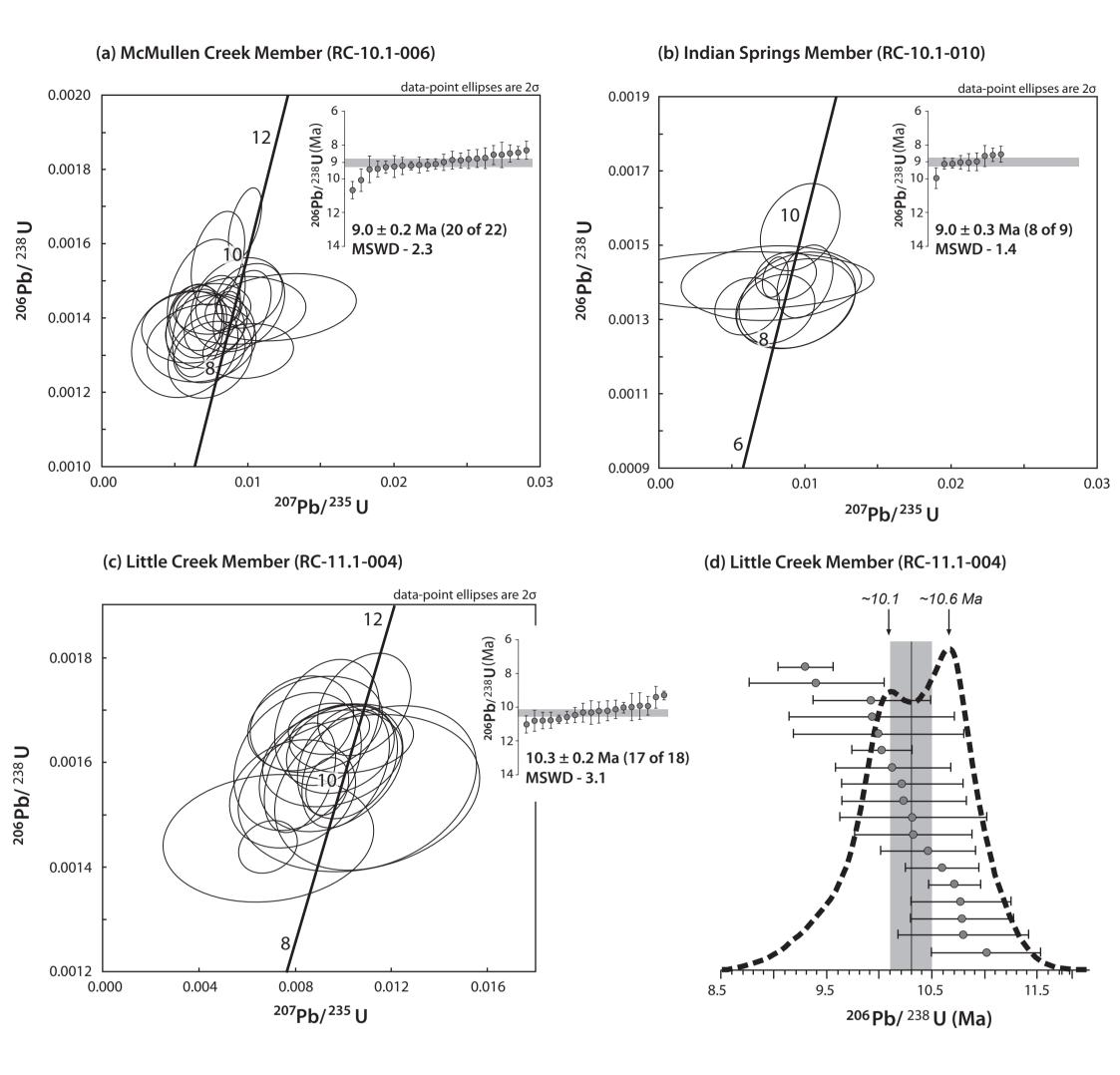
Analysis #

Figure S2i: Dry Gulch Member (ID EK65DB15)

K/Ca

Probability

Age (Ma)



**Figure S3 (a-d).** U-Pb concordia diagrams and weighted average plot for zircon <sup>206</sup>Pb/<sup>238</sup>U ages for: (a) the McMullen Creek Member, (b) the Indian Springs Member, and (c) the Little Creek Member. U-Pb zircon analyses were performed by secondary ion mass spectrometry (SIMS) on a Cameca IMS 1270 ion microprobe located at the University of Edinburgh. (d) Age-probability distribution plot of the Little Creek Member implying the presence of two age populations at ~10.1 Ma and ~10.6 Ma.